Journal Pre-proofs

Research paper

Impurity profiling of PEGylated myristoyl diglyceride, DMG-PEG 2000, a functional excipient used in mRNA lipid nanoparticle formulations

Benedikt Sperber, Marcus Gutmann, Josef Kehrein, Tessa Lühmann, Ulrike Holzgrabe, Lorenz Meinel

PII: S0939-6411(25)00139-0
DOI: https://doi.org/10.1016/j.ejpb.2025.114762
Reference: EJPB 114762

To appear in: *European Journal of Pharmaceutics and Biopharmaceutics*

Received Date: 31 March 2025
Revised Date: 19 May 2025
Accepted Date: 3 June 2025

Please cite this article as: B. Sperber, M. Gutmann, J. Kehrein, T. Lühmann, U. Holzgrabe, L. Meinel, Impurity profiling of PEGylated myristoyl diglyceride, DMG-PEG 2000, a functional excipient used in mRNA lipid nanoparticle formulations, *European Journal of Pharmaceutics and Biopharmaceutics* (2025), doi: https://doi.org/10.1016/j.ejpb.2025.114762

Impurity profiling of PEGylated myristoyl diglyceride, DMG-PEG 2000, a functional excipient used in mRNA lipid nanoparticle formulations

Benedikt Sperber,[a] Marcus Gutmann,[a] Josef Kehrein,[a] Tessa Lühmann,[a] Ulrike Holzgrabe,[a,*] Lorenz Meinel[a,b]*

[a] Institute for Pharmacy and Food Chemistry, University of Wuerzburg, Am Hubland, 97074 Wuerzburg, Germany

[b] Helmholtz Institute for RNA-based Infection Research (HIRI), Josef-Schneider-Strasse 2, 97080 Wuerzburg, Germany

*Corresponding authors: Prof. Dr. Ulrike Holzgrabe and Prof. Dr. Dr. Lorenz Meinel, Institute for Pharmacy and Food Chemistry, University of Wuerzburg, Am Hubland, DE-97074 Wuerzburg, Germany, E-Mail: ulrike.holzgrabe@uni-wuerzburg.de and lorenz.meinel@uni-wuerzburg.de.

Abstract

Lipid nanoparticles have gained significant attention during the COVID-19 pandemic, particularly due to their role in mRNA vaccine delivery. However, their rapid advancement has outpaced the development of established harmonized protocols for the quality control of the various excipients. In this study, we focused on the "stealth" lipopolymer 1,2-dimyristoyl-*rac*-glycero-3-methoxypolyethylene glycol-2000 (DMG-PEG 2000), a critical excipient used in Moderna's Spikevax® mRNA vaccine. We investigated different commercial batches of DMG-PEG 2000 for impurities originating from both synthesis and degradation. Synthesis-related impurities include free glycerol and fatty acids of varying chain lengths, while degradation products result from single or double hydrolysis reactions. These synthetic and degradation-related impurities were primarily analyzed using an optimized high-performance liquid chromatography method with a charged aerosol detector (HPLC-CAD). Applying this validated method, a high purity of commercially available DMG-PEG 2000 was revealed, with every batch investigated exceeding a purity of 98.5%. In addition, gas chromatography (GC), HPLC with an evaporative light scattering detector (HPLC-ELSD), and matrix-assisted laser desorption/ionization time-of-flight (MALDI-TOF) mass spectrometry were employed for comparative purposes and to enable further characterization. Based on these analyses, we developed a streamlined and robust impurity profiling protocol that (i) provides essential insight into the impurity profile of DMG-PEG 2000 in marketed products and (ii) may facilitate more decentralized and standardized validation processes in the future. The analytical approach presented here may also serve as a foundation for a future pharmacopeial monograph proposal for DMG-PEG 2000.

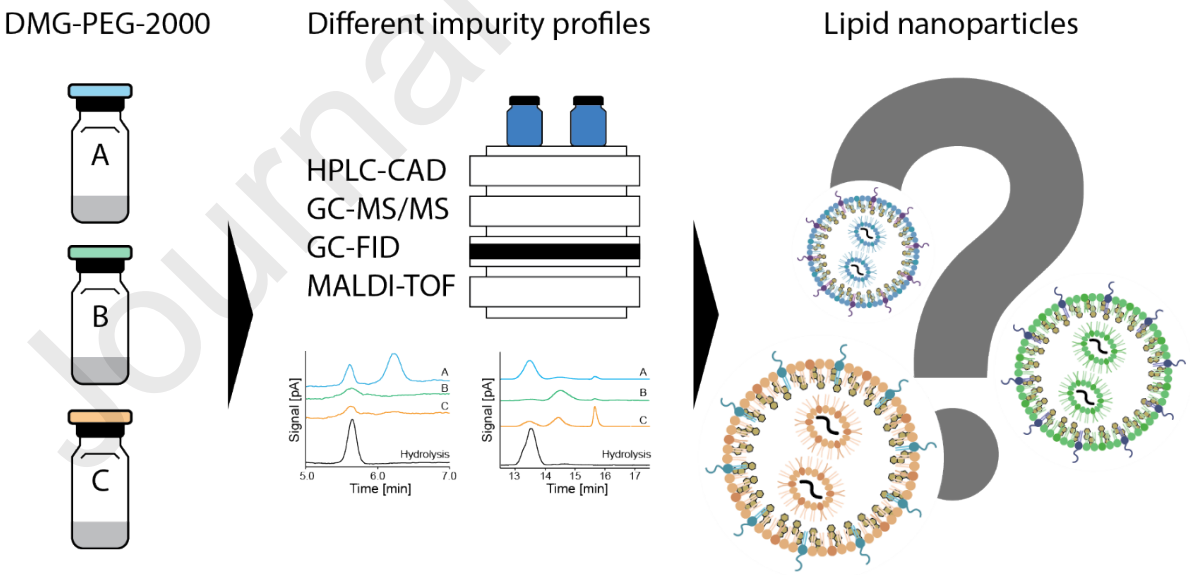

Keywords: Charged aerosol detector; degradation; high-performance liquid chromatography; lipid nanoparticle; poly(ethylene glycol)

1 Introduction

With the advent of Onpattro, Comirnaty, and Spikevax, lipid nanoparticles (LNPs) have demonstrated their potential to revolutionize non-viral gene delivery. This is reflected by many more LNP-based strategies being actively developed [1, 2], rationalized [3], and investigated in clinical trials – including novel therapies against viral infections, cancer, and genetic disorders [4]. However, the highly complex nature of LNPs should raise concerns about their composition, specifically the types of lipids administered, including impurities from synthesis and degradation products of individual molecules, the LNP formulation, and storage conditions. LNPs are usually composed of (i) phospholipids, providing structural integrity, (ii) sterols, modulating membrane rigidity, (iii) ionizable cationic lipids, enabling mRNA encapsulation, and (iv) "stealth"-inducing poly(ethylene glycol) (PEG)-based lipopolymers that regulate the LNP size by establishing a hydrophilic "corona" on the particle surface [5]. All these excipients may degrade and vary in their composition across different suppliers and batches, affecting both drug safety and efficacy [6]. In this regard, classifying these lipids merely as excipients is debatable. For example, the stealth lipid used in the Moderna vaccine, 1,2-dimyristoyl-*rac*-glycero-3-methoxypolyethylene glycol-2000 (DMG-PEG 2000), was approved by the FDA as "starting material for the drug substance" but as excipient by the EMA [7]. While both agencies require the identification and quantification of such lipid species, deemed as critical quality attributes [8], the inconsistency of regulatory scrutiny potentially imposes high barriers pushing these towards the registration requirements of active pharmaceutical ingredients [9]. The current situation highlights the urgent need to strive for a quality control process of novel lipidic LNP constituents that is consistent, harmonized, and readily-performable – akin to existing compendial monographs for excipients described in many pharmacopeias across the globe.

High-performance liquid chromatography (HPLC) is the gold standard for the analysis in pharmaceutical quality control and resembles an integral part of many drug monographs. It is more cost-effective than e.g. liquid chromatography-mass spectrometry (LC-MS) [8] and has been used for various lipid types [10-13]. HPLC also allows for the implementation of different detectors for non-chromophoric compounds, including, by nebulization of the eluent and evaporation of solvent, charged aerosol (CAD) [13] and evaporative light scattering detectors (ELSD) [14]. Both are able to detect non-volatile substances, such as lipids, based on charge and light scattering, respectively [8].

Therefore, we set out to develop a routine HPLC analysis protocol for a key LNP lipid: DMG-PEG 2000 of the Moderna vaccine (**Figure 1**). We evaluated impurities derived from synthesis and degradation products resulting from hydrolysis. We considered the analytical profiles of these impurities (**Figure 1B**) with chromatograms obtained from commercially available DMG-PEG 2000 samples of different suppliers to optimize the HPLC separation performance. Lastly, we integrated the validated HPLC methods along with other methods, including ultra-high-performance liquid chromatography for the identification of free glycerol and gas chromatography coupled with mass spectrometry for the profiling of fatty acids, to provide a draft monograph for possible use in the major pharmacopeias.

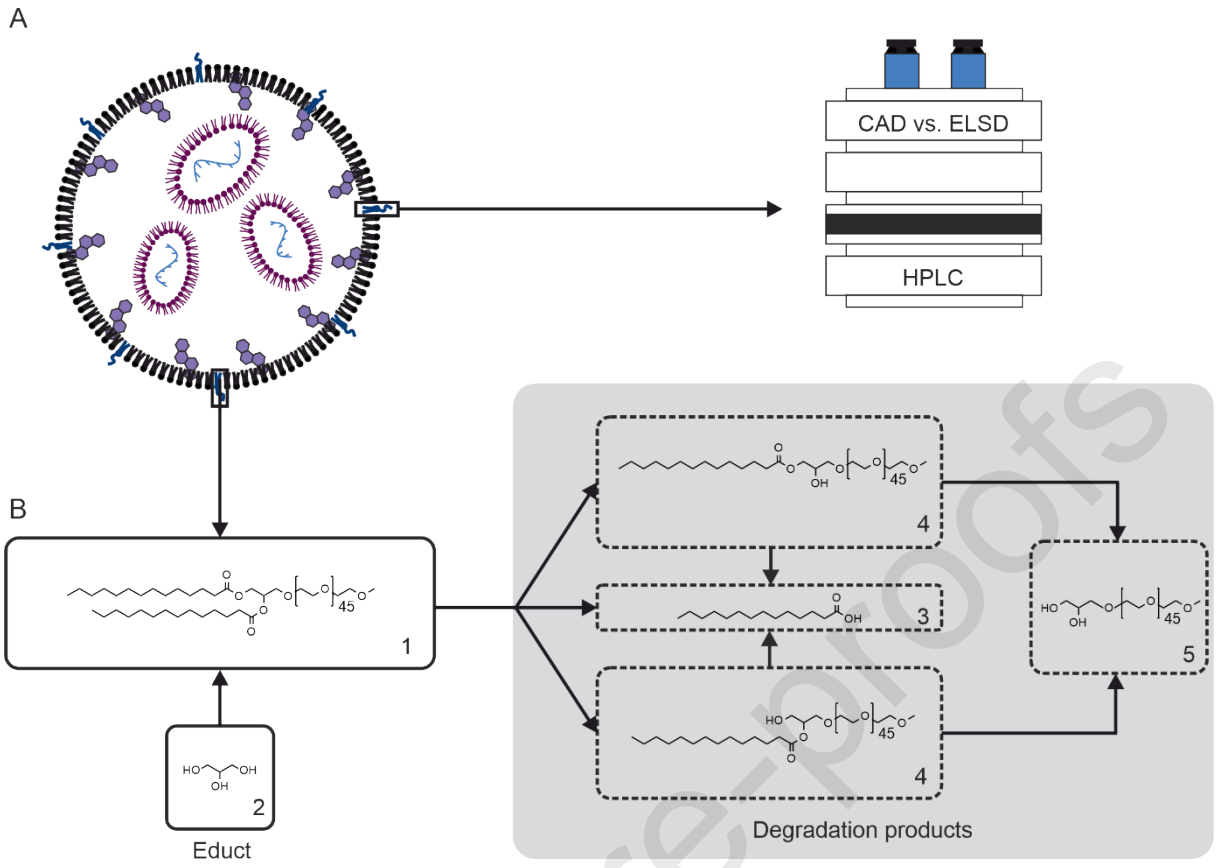

Figure 1: HPLC analysis of DMG-PEG 2000, used for the Spikevax COVID-19 mRNA vaccine of Moderna. (A) Schematic illustration of the Spikevax mRNA vaccine (50:10:38.5:1.5 molar ratio of SM-102, distearoylphosphatidylcholine, cholesterol, and DMG-PEG 2000) and the applied HPLC analysis methods. (B) DMG-PEG 2000 and the expected impurity profile, derived from synthesis educts and degradation products (1 = DMG-PEG 2000; 2 = glycerol; 3 = myristic acid; 4 = PEGylated monomyristin; 5 = PEGylated glycerol). We systematically evaluated various HPLC settings and different detectors to optimize the separation performance for the relevant compounds.

2 Materials and methods

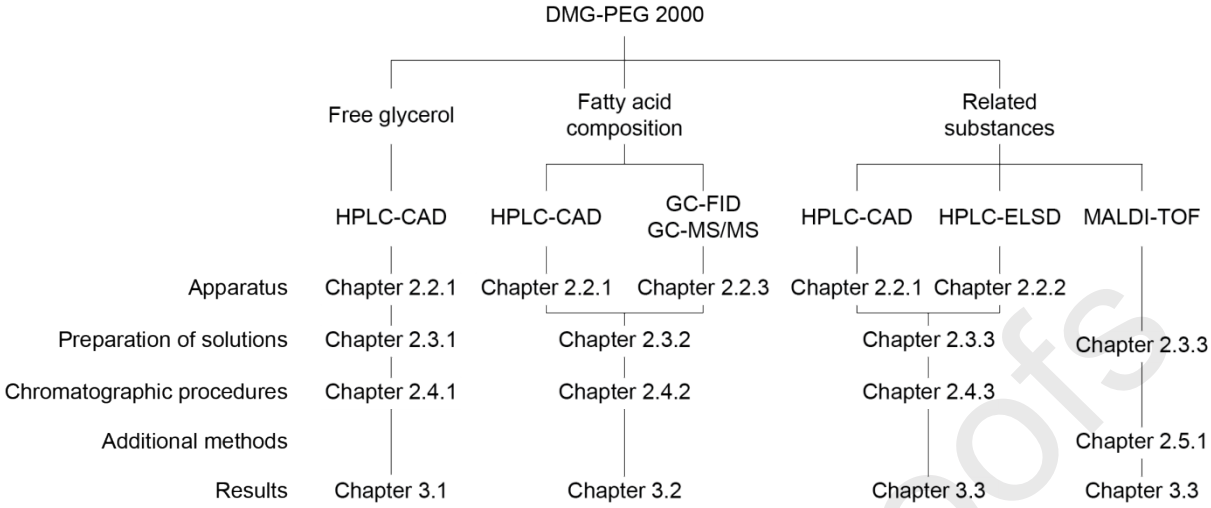

Figure 2: Analytical workflow for DMG-PEG 2000

2.1 Reagents and chemicals

All chemicals were of analytical grade unless stated otherwise. PEGylated glycerol (**Figure 1B**: **5**) was purchased from Alfa Chemicals Co., Ltd (Zhengzhou City, China). Formic acid, lauric acid, linoleic acid, α-linolenic acid, myristic acid, palmitic acid, palmitoleic acid, oleic acid, and stearic acid (all <99%), as well as *rac*-glycerol-1-myristate (1-monomyristin), 1,2-dimyristoyl-*rac*-glycerol (DMG), benzoyl chloride, 1,2,4-butanetriol, glycerol, hexane, heptane, sodium hydroxide, sodium chloride, sodium sulfate, hydrochloric acid, boron trifluoride-methanol solution, and methyl *tert*-butyl ether were purchased from Sigma Aldrich (Taufkirchen, Germany). A fatty acid methyl ester mixture according to [15] was purchased from Sigma Aldrich. LC-MS grade methanol, acetonitrile, tetrahydrofuran, and water were also purchased from Sigma Aldrich. DMG-PEG 2000 (**Figure 1B**: **1**) samples were from Cayman Chemicals Company (Ann Arbor, United States), Avanti Polar Lipids, Inc. (Alabaster, United States), and Evonik Industries AG (Hanau, Germany). 1,2-distearoyl-*rac*-glycerol-PEG 2000 was ordered from Avanti Polar Lipids. The order of the supplier names does not necessarily coincide with the order of the naming scheme used within the manuscript.

2.2 Apparatus

2.2.1 **HPLC-CAD.** HPLC-CAD measurements were performed using a Vanquish™ Flex modular chromatographic system (Thermo Fisher Scientific, Germering, Germany) consisting of a binary pump with online degasser, a thermostatted split sampler, and a column compartment with a passive pre-heater. Detection was carried out in-line on a diode array detector and CAD using nitrogen supplied by an ESA nitrogen generator (Thermo Fisher Scientific). Data acquisition was handled by Chromeleon® 7.3 software (Thermo Fisher Scientific). Specific CAD settings are detailed below (chapter 2.4).

2.2.2 HPLC-ELSD. The HPLC-ELSD experiments were performed on an Agilent 1260 Infinity II HPLC (Agilent Technologies Inc., Waldbronn, Germany) equipped with an automatic vial sampler, a flexible pump, and a multi-column oven. Detection was carried out using an Agilent 1260 Infinity II ELSD supplied with nitrogen. Data acquisition was handled by Agilent ChemStation software. ELSD settings: evaporator and nebulizer temperature at 35 °C, gas flow rate of 1.60 l/min, data collection rate of 40 Hz, and a PMT-Gain of 1.0.

2.2.3 Gas chromatography flame ionization detector (GC-FID) and tandem mass spectrometry (GC-MS/MS). GC-FID and GC-MS/MS experiments were performed using a Trace 1300GC system (Thermo

Fisher Scientific). The injection was 1 µl splitless. After separation on a Supelco® SP-2560 100m x 0.25 mm fused silica capillary column with 0.20 µm film thickness and poly-biscyanopropylsiloxane as stationary phase (Sigma Aldrich), the sample was split using SilFlow™ stainless steel microfluidic platform (Trajan Scientific and Medical, Ringwood, Australia) to enable simultaneous flame ionization detection for quantification and MS/MS detection for identification. The injector temperature was set to 250 °C with the column initially at 120 °C, ramped at 4 °C/min to 240 °C and held for 15 min. Helium (Linde Gas, Pullach, Germany) was used as carrier gas at a constant pressure of 500 kPa. MS detection was performed via electron impact ionization at 70 eV with a transfer line and source temperatures of 250 °C, respectively. A mass range between 100 m/z and 400 m/z was scanned to obtain full-scan mass spectra. The FID temperature was set to 250 °C. Quantification was carried out by normalizing each peak area to the sum of the areas of all peaks, except the peak resulting from the solvent. Peaks with less than 0.05% (the limit of quantification) of the total area were disregarded according to [16, 17]. All measurements were performed in duplicate, due to the very high sample consumption required for this method (approximately 20 times higher than for the HPLC-CAD).

2.3 Preparation of solutions for chromatography

2.3.1 Free glycerol. Glycerol was derivatized by a Schotten-Baumann reaction, using 1,2,4-butanetriol (5 mg/ml in 4 M sodium hydroxide) as internal standard. The derivatization method was modified from [18]. Briefly, 10.0 mg of DMG-PEG 2000 was dissolved in 965 µl 4 M sodium hydroxide, followed by addition of 35 µl internal standard solution. Subsequently, the reaction was initiated by adding 500 µl hexane and 100 µl benzoyl chloride. After vortexing, samples were shaken at 40 °C and 1000 rpm for 4 h. The organic phase containing the benzoyl ester derivatives was collected, washed with 500 µl hexane, dried under nitrogen and reconstituted in 1 ml acetonitrile/water mixture (45:55, v/v) for analysis.

2.3.2 Fatty acid profiling. For LC analysis, saponification was performed as described in [19]. About 15 mg of DMG-PEG 2000 was dissolved in 1 M sodium hydroxide containing 10 % methanol to a final concentration of 1.5 mg/ml and incubated at 40 °C for 6 h. The fatty acid extraction method was modified from [20]. Briefly, 500 µl of saponified solution was acidified with 100 µl formic acid to adjust the pH to 3.2, followed by addition of 500 µl methyl *tert*-butyl ether. The sample was mixed thoroughly and centrifuged for 5 min at 2700 × g. The organic phase was collected, dried under nitrogen and reconstituted in 1 ml acetonitrile/water mixture (75:25, v/v) for analysis.

For GC analysis, sample preparation followed [17], method C. 0.1 g of DMG-PEG 2000 was dissolved in a methanolic solution of sodium hydroxide (20 g/l) and heated under reflux for 30 min. After the addition of 2 ml boron trifluoride-methanol solution (140 g/l), refluxing was continued for another 30 min. Fatty acid methyl esters were extracted with 4 ml heptane under reflux for 5 min. The solution was cooled, and saturated sodium chloride solution was added. The organic phase was collected, washed 3 times with 2 ml water, and dried overnight over anhydrous sodium sulfate. Deviating from the monograph, the organic solution was diluted 1:3 with heptane to avoid column overloading.

2.3.3 Related substances. For method development, 10.0 mg DMG-PEG 2000 was hydrolyzed with 0.05 M aqueous hydrochloric acid solution at 40 °C for 4 h, neutralized with 0.05 M sodium hydroxide and diluted to 1.5 mg/ml with water/acetonitrile (20:80, v/v). Stock solutions of myristic acid (1 mg/ml) and 1-monomyristin (2.5 mg/ml) were prepared in methanol, respectively. Stock solutions of PEGylated glycerol (2.5 mg/ml) and DMG-PEG 2000 (2.5 mg/ml) were prepared in a mixture of water/acetonitrile (20:80, v/v). All stock solutions were stored at -20 °C. Reference solutions (0.05 – 0.25 mg/ml) were prepared by diluting with water/acetonitrile (20:80 v/v); lower concentrations (0.005 – 0.025 mg/ml) were obtained by 1:10 dilution of the respective references.

2.4 Chromatographic procedures

The following section provides a detailed description of the chromatographic procedures. For each procedure, a suggested method for inclusion in a monograph is presented in the Supporting Information (**Tables S1-S3Error! Reference source not found.**).

2.4.1 Free glycerol (Table S1). Free glycerol was determined using an Infinity Poroshell 120, 50 x 2.1 mm, 1.9 µm (Agilent Technologies Inc.) UHPLC column at a flow rate of 0.55 ml/min and an injection volume of 1 µl. The autosampler and column temperatures were 30 °C and 55 °C, respectively. Mobile phase A consisted of water + 0.01% (v/v) formic acid and mobile phase B was acetonitrile. The applied gradient started with a 1 min isocratic step at 45% B, followed by a 5 min linear increase to 60% B, then a 2 min isocratic hold at 60% B, and re-equilibration at 45% B for 2 min. UV detection at 231 nm and CAD detection were used for quantification. CAD settings: evaporation temperature 50 °C, data collection rate 10 Hz, filter constant 3.6 s, and power function value 1.0.

2.4.2 Fatty acid profiling (Table S2). Fatty acid separation was performed on the same UHPLC column for free glycerol (chapter 2.4.1), at a flow rate of 0.4 ml/min. Column and autosampler temperatures were set to 25 °C and 8 °C, respectively. Mobile phases A and B were similar to free glycerol (chapter 2.4.1). The applied gradient started with 2 min at 75% B, followed by a 7 min linear increase to 90% B, a 1 min isocratic hold, and a re-equilibration at 75% B for 3 min. Detection was carried out by CAD. CAD settings: evaporation temperature 25 °C, data collection rate 10 Hz, filter constant 3.6 s, and power function value 1.0.

Additional GC analyses were performed, which represent the method of choice within the European Pharmacopeia [21] and, given the limitations of the HPLC-CAD method (chapter 3.2.2, *vide infra*), were used as basis for the monograph proposal in **Table S2** instead.

2.4.3 Related substances (Table S3). DMG-PEG 2000 and its organic impurities were separated using a reversed-phase (RP) Accucore™ PFP 100 x 4.6 mm, 2.6 µm column (Thermo Fisher Scientific). Columns tested during method development included YMC Triart™ C18 150 x 4.6 mm, 5 µm (YMC Europe GmbH, Dinslaken, Germany), ZORBAX 300SB-CN 150 x 4.6 mm, 5 µm (Agilent Technologies Inc), and Kinetex PFP 100 x 4.6mm, 2.6 µm (Phenomenex Ltd., Aschaffenburg, Germany) column. Gradient elution was applied utilizing water + 0.01% formic acid (v/v) as mobile phase A and acetonitrile as mobile phase B, with the full gradient profile of the optimized method listed in **Table 1**. The method comprised a flow rate of 1 ml/min, column temperature of 40 °C, autosampler temperature of 20 °C, and injection volume of 10 µl. CAD settings: evaporation ttemperature 35°C, a data collection rate 10 Hz, filter constant 3.6 s, and a power function value 1.0.

Table 1: Gradient profile the optimized protocol (corresponding to Method D in chapter 3.3.1).

Time [min]	% B
0-3	20
4-7	40
13-17	55
19-23	95
24-26	100
27-32	20

The resolution between peaks (Rs) was calculated according to **equation 1**, dependent on the retention times t of the respective analyte and the peak width at half height w.

$$R_s = \frac{1.18 * (t_{R2} - t_{R1})}{w_{h1} + w_{h2}} \quad (1)$$

2.5 Additional methods

2.5.1 Matrix-assisted laser desorption/ionization time-of-flight mass spectrometry (MALDI-TOF). Samples for MALDI-TOF were collected from the eluent stream during the related substances method (chapter 2.4.3) at the retention times of DMG-PEG 2000, PEGylated monomyristin (**Figure 1B**: **4**) and PEGylated glycerol (**Figure 1B**: **5**). After lyophilization, samples were reconstituted in 100 µl methanol, and 1 µl was embedded in a matrix consisting of α-cyano-4-hydroxycinammic acid in ternary acid solvent (30:70 [v/v] acetonitrile:water/0.1% trifluoracetic acid). Measurements were performed on an Ultraflex TOF/TOF (Bruker Daltonik, Bremen, Germany). Confirmation of the structures was performed by comparing the m/z values of the polymer in each spectrum corresponding to 45 PEG repeating units, and by evaluating the polydispersity index (PDI) for each spectrum.

2.5.2 Determination of the PDI. In polymer chemistry, the number-average molecular weight M_n represents the statistical average molecular weight of all polymer chains in the sample according to **equation 2**, where M_i is the molecular weight of the chain, and N_i is the respective number of molecules. For MALDI, M_n is calculated according to **equation 3**, where I_i is the intensity of the peak in the spectrum [22, 23]. The weight-average molecular weight M_w gives more emphasis to larger molecules in the sample and is calculated according to **equation 4** or **5** for MALDI. Both M_w and M_n are required to calculate the PDI (**equation 6**). High PDI values in pharmaceutically used polymers may result in substantial batch-to-batch variations in the produced drug products [24-26], highlighting the need for polymers with a narrow PDI.

$$M_n = \frac{\sum (N_i M_i)}{\sum N_i} \quad (2)$$

$$M_n = \frac{\sum (I_i M_i)}{\sum I_i} \quad (3)$$

$$M_w = \frac{\sum (N_i M_i^2)}{\sum (N_i M_i)} \quad (4)$$

$$M_w = \frac{\sum (I_I M_i^2)}{\sum (I_I M_i)} \quad (5)$$

$$PDI = \frac{M_W}{M_N} \quad (6)$$

2.5.3 Correction factors. Correction factors were determined as the reciprocal value of the relative response factors (RRF), defined as follows:

$$RRF = \frac{A_i}{A_s} * \frac{c_s}{c_i} \quad (7)$$

A_i and A_s are the areas of the impurity and the analyte (DMG-PEG 2000), and c_i and c_s are the concentrations of the impurity and analyte, respectively.

3 Results and discussion

We examined the impurities of the LNP lipopolymer DMG-PEG 2000 (**Figure 1B**: **1**) derived from synthesis **Figure 1B**: **2** = glycerol, and **3** = myristic acid) and degradation resulting either from single (**Figure 1B**: **3**, and **4** = PEGylated monomyristin) or double hydrolysis reactions (**Figure 1B**: **3**, and **5** = PEGylated glycerol). First, we investigated the occurrence of free glycerol (chapter 3.1) and fatty acids with varying lengths (cf. chapter 3.2) within commercial samples of DMG-PEG 2000. While free glycerol could be introduced through insufficient PEGylation during synthesis [27] and is determined for other acyl glycerides as well [28-30], accompanying fatty acids could be introduced through an impurity of myristic acid leading to various lipid tail lengths of the stealth lipopolymer. This has been shown to decisively influence shedding of the hydrophilic coating material and, in turn, LNP organ targeting *in vivo* [31, 32]. Similarly, the presence of any unsaturated fatty acid could alter the membrane fluidity and affect LNP stability by possible oxidative degradation during storage and increased binding by serum proteins [33-38]. Afterward, derivatives resulting from hydrolysis were analyzed with an optimized HPLC-CAD protocol and subsequently identified by MALDI-TOF (cf. chapter 3.3).

3.1 *Free glycerol*

3.1.1 Method development. The protocol for the quantification of free glycerol by size exclusion chromatography with an aromatic styrene-divinylbenzene stationary phase [28] was altered: due to commercial unavailability of a column with 7 mm diameter, an Agilent SDV 300 x 8 mm, 5 µm (Agilent Technologies Inc.) was applied. Accordingly, the flow rate and the injection volume had to be adjusted

[16]. Detection was carried out with the CAD (evaporation temperature: 25°C, collection rate 10 Hz, filter constant 3.6 s, power function value 1.0) instead of the refractive index. The altered method resulted in peak asymmetry and low sensitivity for glycerol (**Figure S1A**). Based on the polarity of glycerol, hydrophilic interaction LC on an Accucore™-150-Amide-HILIC (150 x 4.6 mm, 2.6 µm, Thermo Fisher Scientific) column with CAD detection (evaporation temperature: 25°C, collection rate 10 Hz, filter constant 3.6 s, power function value 1.0) was evaluated (Costa et al., 2019; Fontes et al., 2016). Applying an isocratic hold at 95% acetonitrile for 3 min followed by a linear gradient to 40% acetonitrile (mobile phase A: water + 0.01% formic acid [v/v]), glycerol exhibited acceptable peak symmetry but showed an extensive peak overlap with DMG-PEG 2000 (**Figure S1B**).

Due to insufficient performance of the described methods, a derivatization of glycerol using benzoyl chloride (Schotten-Baumann reaction) followed by separation on a RP-C18 column was evaluated as final approach (**Figure S2**) (Frieler et al., 2009; Li et al., 2006). Therefore, DMG-PEG 2000 was hydrolyzed and derivatized (**Figure S2B**), while 1,2,4-butanetriol was selected as internal standard. The developed method was further validated according to ICH Q2(R2).

3.1.2 Validation. For validation of specifity, a 10 mg/ml solution of DMG-PEG 2000 spiked with 0.15% glycerol and internal standard was hydrolyzed and derivatized – the resulting benzoylated glycerol and benzoylated 1,2,4-butanetriol were baseline-resolved for both CAD and UV detection at 231 nm (**Table 2**, specificity and **Figure S2C**). A high linearity for both UV and CAD detector was determined by measuring derivatized glycerol samples with concentrations ranging between 0.05 and 0.3% relative to a 10 mg/ml DMG-PEG 2000 test solution (**Table 2**, linearity). Limit of detection (LOD) and limit of quantification (LOQ) values were determined based on a signal-to-noise ratio of 3 and 10, respectively, with UV detection being approximately two times less sensitive than CAD (**Table 2**, sensitivity). Subsequently, three levels of spiked test solutions were investigated (0.075, 0.175, and 0.275%, $n = 3$). Of note, difficulties arose from benzoylated variants of DMG-PEG 2000 accumulating between the aqueous and organic phases as gel-like substance (**Figure S2B**) during collection of the organic phase (cf. chapter 2.4.1). However, overall, CAD showed smaller relative standard deviations and higher recovery rates compared to UV detection (**Table 2**, repeatability and accuracy) and was thus selected as detector for quantification of glycerol in commercial DMG-PEG 2000 samples.

Table 2: Validation of the quantification of free glycerol by derivatization according to ICH Q2(R2), comparing UV to CAD detection.

Criteria	**Parameter**	**UV (231 nm)**	**CAD**
Specificity	R_s	1.92	1.57
Linearity	R^2 (equation)	0.9995 (y=0.5951x+0.0070)	0.9995 (y=0.5148x+0.0364)
Sensitivity	LOQ	104.3 pg	53.2 pg
	LOD	31.3 pg	16.0 pg
Repeatability	Relative standard deviations	0.6 – 2.9%	0.9 – 1.6%
Accuracy	Recovery	82.7 – 86.5%	82.7 – 90.5%

3.1.2 Sample analysis. Using the validated method, we finally investigated 5 DMG-PEG 2000 samples by 3 different suppliers. Glycerol was below the LOD for all suppliers and batches. Hence, no residual glycerol was detected in commercially available DMG-PEG 2000.

3.2 *Fatty acid profiling*

3.2.1 Method development. We investigated the occurrence of fatty acids of varying lengths by both GC and HPLC-CAD. Suitability of the GC method was first evaluated using a 2 µg/µl solution of fatty acid methyl esters according to [15]. Despite the peak for methyl caproate (C6) merging with the injection peak, the resolution between all analytes was higher than 4.0 rendering the GC method suitable for the profiling of fatty acid compositions.

Alternatively, HPLC-CAD can be used to determine the fatty acid composition in excipients like polysorbate 80 [19, 39, 40]. Advantages over GC include easier sample preparation and the possibility to detect thermolabile ethoxylated or epoxylated fatty acids. However, fatty acids shorter than myristic acid are not detectable by CAD due to their volatility [41]. Striving for an easy-to-follow setup, we adjusted the previously applied method to be used with UHPLC [19, 39]. A quality control solution containing 0.05 mg/ml lauric acid, myristic acid, α-linolenic acid, palmitoleic acid, linoleic acid, palmitic acid, oleic acid and stearic acid was separated with $R_s > 1.8$ for all peaks (**Figure S3, Table S4**).

3.2.2 Sample analysis. First, we investigated 4 batches of 3 different suppliers by GC (**Table 3**). For comparison, one batch of 1,2-distearoyl-*rac*-glycerol-PEG 2000 was analyzed because of the molecule's structural similarity to DMG-PEG 2000 (stearic acid vs. myristic acid as lipid tail). All commercial batches of DMG-PEG 2000 exceeded a 97% content in myristic acid and the batch of 1,2-distearoyl-*rac*-glycerol-PEG 2000 (DSG-PEG 2000) a 99% content in stearic acid, indicating overall high purity. The most prominent alternative fatty acid was behenic acid (C22:0). A small peak was detected for all samples at the same retention time (**Table 3**, "unidentified"), eluting right after the peak assigned to the C22 fatty acid, we hypothesize that this peak could correspond to a C23 fatty acid.

Using the alternative HPLC-CAD method, we further analyzed 5 batches of 3 different suppliers and one additional batch of distearoyl-*rac*-glycerol-PEG 2000 (**Figure S3**). No peaks besides for myristic acid and stearic acid for DMG-PEG 2000 and DSG-PEG 2000 were found, respectively, corroborating our observations from GC. Thus, given a uniform length of the lipid tails, the lipopolymers from different suppliers are expected to be incorporated into the LNP membrane in a similar fashion, a factor determining shedding of the hydrophilic "corona" *in vivo* [31, 32].

Table 3: Fatty acid profiles obtained by GC for commercially available batches of DMG-PEG 2000, including an analogous measurement for 1,2-distearoyl-*rac*-glycerol-PEG 2000.

Analyzed sample	C8 [%]	C10 [%]	C14 [%]	C16 [%]	C18 [%]	C20 [%]	C22 [%]	unidentified [%]
1,2-distearoyl-*rac*-glycerol-PEG 2000				0.09	99.26		0.56	0.10
Batch A1			98.97	0.06	0.28		0.70	
Batch A2			98.17			0.11	1.65	0.07

Batch B2	0.45	0.18	97.42	0.06	0.1		1.52	0.24
Batch C1			98.23				1.69	0.08

3.3 *Impurity profiling of related substances*

After determination of free glycerol and fatty acids, we focused on the optimization of a HPLC-CAD method for the detection of hydrolysis products of DMG-PEG 2000, including myristic acid, PEGylated monomyristin and PEGylated glycerol (**Table 4**).

Table 4: Analytes and structures of related substances in DMG-PEG 2000, with labels for peak assignments listed in accordance with the labeling scheme found in **Figure 1**.

Analyte	Structure	Peak assignment
DMG-PEG 2000	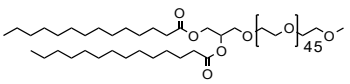	1
DMG	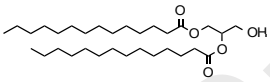	1a
Myristic acid	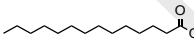	3
PEGylated monomyristin	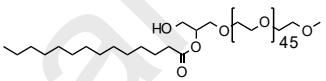 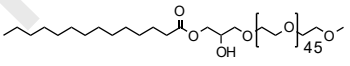	4
1-monomyristin	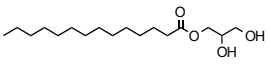	4a
PEGylated glycerol	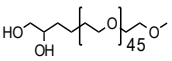	5

3.3.1 Method development. We first evaluated 3 stationary phases with varying polarity to tune the influence of the hydrophilic polymer chain of **1** on retention time: a hydrophobic RP-18 (YMC Triart™ C18 150x4.6 mm, 5 µm), as well as mid-polar cyano (ZORBAX 300SB-CN 150x4.6 mm, 5 µm) and pentafluorophenyl columns (Accucore PFP 100 x 4.6 mm, 2.6 µM). For evaluation, a reference solution for selectivity testing (ICH Q2R2 [42]) containing 0.2 mg/ml **1**, **1a**, **3**,**4a** and **5** was dissolved in methanol. 1-monomyristin was applied as surrogate for **4**, while DMG was introduced to investigate the influence of PEG. Using varying gradients, broad peaks for **5** and DMG-PEG 2000 on the RP18 and for DMG-PEG

2000 on the cyano column were observed, thereby rendering the pentafluorophenyl column as best choice (**Figure S4**).

Regarding the mobile phase, both with the Accucore PFP 100 x 4.6 mm and an alternative Kinetex pentafluorophenylpropyl column (100 × 4.6 mm, 2.6 µm) we observed significant baseline fluctuations using varying proportions of methanol as mobile phase B, as reported previously [43], resulting in an overlap of the peaks for the blank injection and **4**. This was resolved by exchanging methanol entirely with acetonitrile (**Figure S5**). For optimization of the gradient setting, separation was assessed with 10 mg/ml samples obtained by hydrolysis of 1 g of DMG-PEG 2000. Two-step gradients with different isocratic holds and steepness were assessed based on peak shapes, resolutions, and separations leading to the detection of unknown impurities A and B within samples of Suppliers A and B, respectively (Methods A, B, and C, **Figure S6**). Ultimately, an additional isocratic step led to final Method D, characterized using a spiked solution merged from samples of Supplier A and B (**Figure 3A-C**). This method could not be optimized further and was thus deemed as best choice for profiling of related substances.

3.3.2 Choice of detector. For further investigation, we replaced the CAD in the optimized Method D with an ELSD, reflecting the broader availability of the detector. Compared to CAD, showing ≥ 0.9995 R^2 values for linear regressions on dilution series of **4**, **3**, and **1** in a concentration range of 0.5 – 2.5% (m/m, relative to a test solution of 10 mg/ml) [44, 45], the ELSD showed ≥ 0.9995 R^2 values only for quadratic regressions (**Figure 3D-F**, **Table S5**). Furthermore, CAD was overall more sensitive (**Table S6**), being able to quantify impurities below 0.05% (m/m), the threshold specified for active pharmaceutical ingredients by [46, 47]. Thus, the CAD was classified as superior detector.

3.3.3 Evaporation temperatures and inverse gradients. In addition, detection at 25 °C, as well as applying an inverse gradient at 25 °C were implemented in Method D. **3** is semi-volatile, which impacts the uniformity of response at higher evaporation temperatures [19, 41, 48]. Furthermore, an inverse gradient with a secondary pump can maintain a constant solvent composition at the CAD minimizing the gradient's impact on the response [49, 50]. Therefore, based on additional dilution series in concentration ranges of 0.5 – 2.5% and 0.05 – 0.25% for **1**, **3**, **4**, and **5**, correction factors for these settings were evaluated (**Table S7**, **Figure S7**). With the inverse gradient, uniformity increased for lower concentrations of **4a** and **5** but decreased for myristic acid. Evaporation at 35 °C showed correction factors near 1 at both working ranges for **4a** and **5**, and response was uniform with **1**. However, **3** exhibited a weaker response. Despite the lower signal of the semi-volatile **3**, 35 °C was the preferred option due to the results for **4a** and **5**. The inverse gradient was not further investigated at 35 °C, as it showed a negative impact on the correction factor of myristic acid at 25 °C.

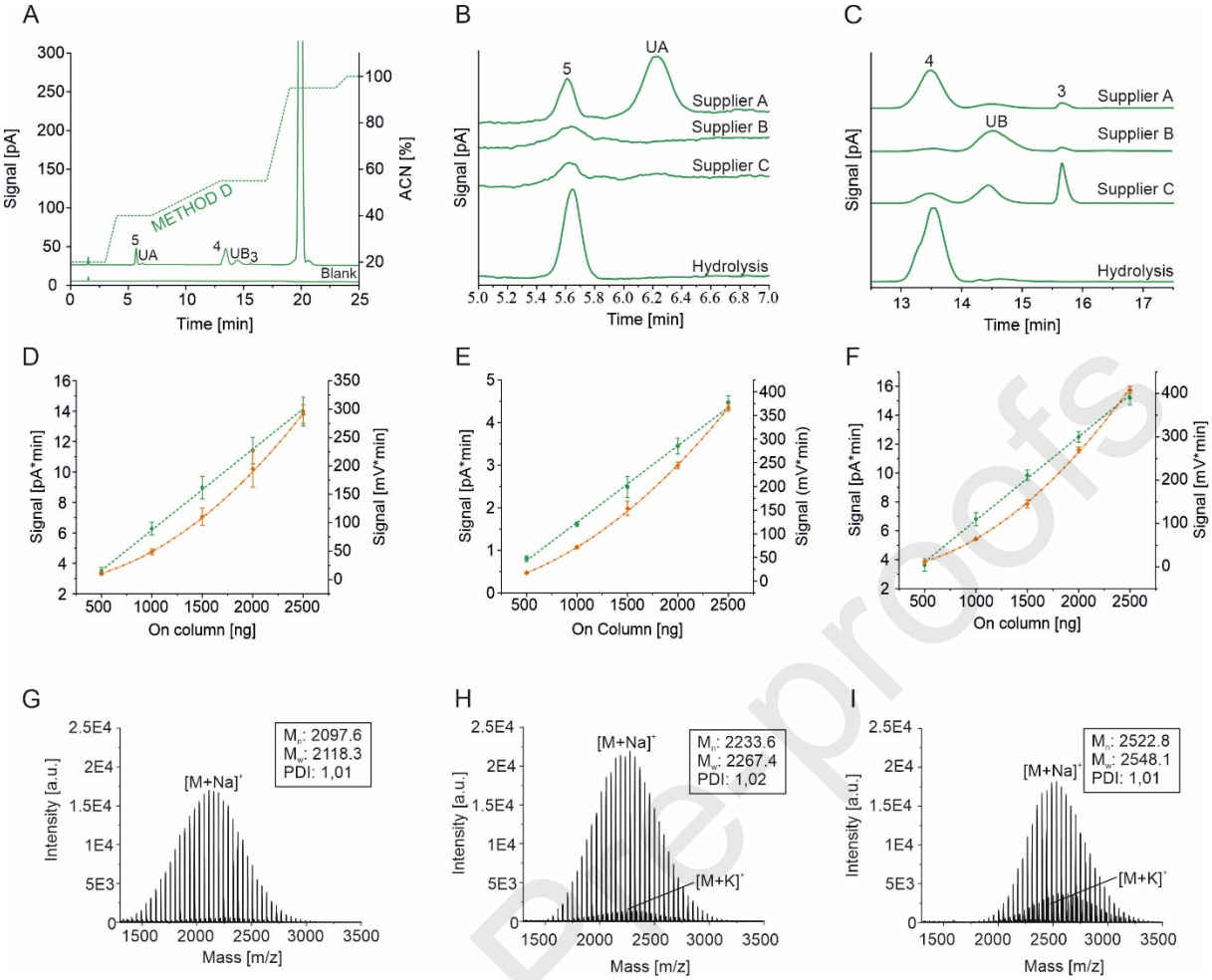

Figure 3: Separation performance of the developed HPLC-CAD method D, detector comparison, and MALDI-TOF analysis. (A) Gradient profile and chromatogram of a 20 mg/ml DMG-PEG 2000 (composed of 10 mg/ml of samples from Supplier A and Supplier B respectively, to cover the whole impurity profile) spiked with 0.15% (m/m) **5** and **3**. (B-C): Enlargement of chromatograms for samples of different suppliers (10 mg/ml) shown for (B) 5-7 min and (C) 13-17 min retention intervals. (D-F) Regression lines for the ELSD (orange) and the CAD (green) covering a range of 0.5 – 2.5% for (D) **5**, (E) **3,** and (F) **1**. (G-I) MALDI-TOF spectra of (G) **5**, (H) **4**, and (I) **1** from Supplier B, with the respective M_n and M_w values in g/mol, as well as the PDI. Peak labels correspond to the labeling scheme in **Figure 1**, **UA**: unknown impurity A; **UB**: unknown impurity B.

3.3.4 Peak assignment by MALDI-TOF. Compounds separated by the final Method D were further identified by MALDI-TOF MS (**Figure 3G-I**, shown exemplarily for Supplier B, **Table 5**, listed for Supplier A and B) and calculation of the PDI. Polar polymers such as PEG usually form single positively charged ions, $[M+H]^+$, $[M+Na]^+$, or $[M+K]^+$ [51, 52]. We observed dominant peaks for $[M+Na]^+$, with noticeable additional $[M+K]^+$ peaks for **1** and **4**. Regarding Supplier A, the calculated mass differences of **4** and **5** to **1** were 210.17 and 420.38 g/mol, respectively, corresponding to the cleavage of one or two myristic acid sidechains. PDI values derived from calculated M_n and M_w values were 1.01 or 1.02 for all compounds suggesting low polydispersity. Overall, all compounds identified by MALDI-TOF corresponded to the expected molecules, validating our peak assignment. However, we were unable to manually collect and subsequently analyze the detected unknown impurities A and B by MALDI-TOF, as achieved for DMG-PEG 2000 and its degradation products. A discussion on the possible identity of impurity B can be found in chapter 3.4.2 (*vide infra*).

Table 5: Results of MALDI measurements for Supplier A and B.

Structure	m/z calculated (n=45, $[M+Na]^+$)	m/z observed (n=45, $[M+Na]^+$)	Difference to DMG-PEG 2000 (n=45)	M_n [g/mol]	M_w [g/mol]	PDI
Supplier A						
DMG-PEG 2000 (1)	2576.23	2575.56		2498.63	2513.91	1.01
PEGylated monomyristin (4)	2365.87	2365.39	210.17	2274.45	2293.49	1.01
PEGylated glycerol (5)	2155.52	2155.18	420.38	2038.62	2057.20	1.01
Supplier B						
DMG-PEG 2000 (1)	2576.23	2575.64		2522.79	2548.07	1.01
PEGylated monomyristin (4)	2365.87	2365.46	210.18	2233.61	2267.45	1.02
PEGylated glycerol (5)	2155.52	2155.18	420.46	2097.59	2118.33	1.01

3.4.2 Validation. Applying Method D on the merged solution (**Figure 3A-C**), all analytes were visually baseline-resolved indicating sufficient specificity (R_s = 1.80 between unknown impurity A and **5**, R_s= 1.30 for **4** and unknown impurity B, and 1.84 between unknown impurity B and **3**). As discussed in the method development section (3.3.1), while the resolution between **4** and unknown impurity B was below the specified threshold of 1.5 for baseline resolution [16], the separation was considered acceptable due to the polymeric analytes resulting in large peak widths (**equation 1**) and an absence of further improvement in the separation when adjusting either the gradient or the mobile phase composition.

Linearity was determined for **1**, **3**, **4a** and **5**. **4** was commercially unavailable and a contract synthesis was unsuccessful. Two chemicals were investigated to serve as surrogate for **4**: PEG 2000-myristic acid and 1-monomyristin (**Figure S8A**). PEG 2000-myristic acid exhibited a poor peak shape while 1-monomyristin eluted with a sharp peak approximately between **4** and unknown impurity B (**Figure S8B**). Thus, the latter was selected to function as surrogate for linearity, inter-day precision and accuracy investigation. We detected sufficient linearity ($R^2 \geq 0.99$, **Table 6**, **Figure S7C,F**) for high and low working ranges (0.5 – 2.5% and 0.05 – 0.25% relatively to a 10 mg/ml sample of DMG-PEG 2000, respectively).

Table 6: Linearity results for DMG-PEG 2000 and its impurities.

High working range		
Analyte	**R^2**	**Equation**
DMG-PEG 2000 (1)	0.998	y=0.00053x+0.9474
Myristic acid (3)	0.998	y=0.0014x+0.0301
1-monomyristin (4a)	0.998	y=0.0059x+1.0378
PEGylated glycerol (5)	0.999	y=0.0052x+0.9930
Low working range		
Analyte	**R^2**	**Equation**
DMG-PEG 2000 (1)	0.999	y=0.0082x+0.0182
Myristic acid (3)	0.996	y=0.0013x+0.0222
1-monomyristin (4a)	0.999	y=0.0082x+0.0125
PEGylated glycerol (5)	0.998	y=0.0082x+0.0328

Inter-day precision and accuracy were evaluated at three concentration levels (0.05%, 0.10%, and 0.15% of the test solution) for **3**, **4a** and **5** as well as three modified levels (0.5%, 1.5%, and 2.5%) for **4a** and **3** because of their higher concentrations in commercial batches – all measurements showed a satisfiable accuracy and precision (cf. **Table S8**). The LOQ value for **4a** was not evaluated as it resulted in a sharp peak – in contrast, **4** showed a broad peak, possibly due to its polydispersity. Therefore, LOQ values for this surrogate could not reflect the LOQ of **4**. Overall, however, both impurities, polydisperse **5** as well as semi-volatile **3**, were quantifiable below the reporting threshold of 0.05% (**Table S9**).

Summarizing our validation regarding commercial samples (**Table 7**), the most notable differences between Supplier A and Supplier B were observed for **4** and unknown impurity B. Supplier A showed high levels of **4** (1.09% and 1.21%, respectively), whereas Supplier B contained only trace amounts of this degradation product. Conversely, unknown impurity B reached up to 0.33% in Supplier B's batches but was only detectable near the LOQ for Supplier A. Interestingly, Supplier C showed significant amounts of both **4** and unknown impurity B and was the only supplier with substantial amounts of **3** (1.02%).

Overall, while the impurity profiles varied between suppliers, batch-to-batch variation within each supplier remained relatively low, with DMG-PEG 2000 samples showing high purity across all sources. Still, while impurities did not exceed 1.35% within the analyzed batches, the presence of **4** and the detected unknown impurities A and B at least raise a point for discussion about their possible pharmacokinetic influence on the *in vivo* fate of LNP formulations upon higher degrees of contamination. For example, **4** could be integrated into the outer LNP membrane and influence important properties such as the hydrodynamic diameter. In fact, DMG-PEG 2000 was previously systematically compared to various monoacyl derivatives, comparable to **4**. LNP formulations using these variants resulted in larger LNPs and higher *in-vitro* transfection efficiency [53]. Generally, variations in the content of PEGylated stealth lipids have been shown to influence particle size, LNP fusion, and loading of mRNA [54, 55]. Follow-up studies may assess a possible contribution of the detected impurities to such effects.

Due to the hydrogen-bonding and dipole-dipole interaction capabilities of pentafluorophenyl columns, we hypothesize that the peaks for **4** and the unknown impurity B correspond to structural isomers, hence PEGylated 1- and 2-monomyristin (**Figure 1B: 4**, top vs. bottom). A hydrolytic cleavage either at position 1 or 2 would result in a terminal or a central hydroxyl group within the glycerol backbone, respectively. These hydroxyl groups could thus differ in their solvent-exposure leading to variations in interactions with the stationary phase. This is further supported by the almost identical peak shapes and widths, as well as similar retention times.

Table 7: Impurity profiling for commercially available DMG-PEG 2000 batches by different suppliers.

Supplier and Batch	Unknown impurity A [%]	**5** [%]	**4** [%]	Unknown impurity B [%]	Myristic acid	Total impurities [%]	Purity [%]
Supplier A Batch 1	0.035	<LOQ	1.09	0.034	<LOQ	1.16	98.84
Supplier A Batch 2	0.036	<LOQ	1.21	0.033	<LOQ	1.27	98.73
Supplier B Batch 1	<LOQ	<LOQ	0.034	0.318	0.097	0.45	99.55
Supplier B Batch 2	<LOQ	<LOQ	0.036	0.327	0.108	0.47	99.53
Supplier C Batch 1	<LOQ	<LOQ	0.12	0.213	1.02	1.35	98.65

4 Conclusions and outlook

In this study, we established a robust impurity profiling protocol for the stealth lipopolymer DMG-PEG 2000, a key excipient in the Moderna mRNA vaccine. Using optimized HPLC conditions – including tailored stationary and mobile phases – we successfully developed an analysis protocol to sufficiently separate the relevant synthetic and degradation-related impurities across samples from different commercial suppliers. Our analysis confirmed the absence of free glycerol or alternative fatty acids

indicating a high level of purity of commercially available samples. Nonetheless, two unknown impurities were consistently observed. While their exact structures remain unresolved, preliminary evidence suggests that they may represent structural isomers formed via partial hydrolysis. Further investigation will be required to elucidate their identities and assess potential implications for product quality and regulatory assessment. While recent studies have reported on the HPLC analysis of whole LNP lipid mixtures [56, 57], including those containing DMG-PEG 2000 [58], our analytical workflow including HPLC-CAD and GC was designed to support research and future pharmacopeial monograph development for standardized excipient quality control.

CRediT authorship contribution statement

Benedikt Sperber: Investigation, Formal analysis, Methodology, Validation, Visualization, Writing - original draft. Marcus Gutmann: Writing - review & editing. Josef Kehrein: Writing - original draft, Writing - review & editing. Ulrike Holzgrabe: Writing - review & editing. Tessa Lühmann: Conceptualization, Supervision. Lorenz Meinel: Conceptualization, Supervision, Formal analysis, Data curation, Funding acquisition, Writing - review & editing.

Funding

This work was funded by the BMWK (Bundesministerium für Wirtschaft und Klimaschutz) within the BASE-Lipid consortium (FKZ: 16LP401002).

Declaration of competing interest

The authors have no conflicts of interest to disclose.

Acknowledgments

We gratefully acknowledge Evonik for supplying us with DMG-PEG 2000.

Supplementary materials

Supplementary material associated with this article can be found in the online version.

Data availability

Data will be made available on request.

References

[1] R. Masarwy, D. Breier, L. Stotsky-Oterin, N. Ad-El, S. Qassem, G.S. Naidu, A. Aitha, A. Ezra, M. Goldsmith, I. Hazan-Halevy, Targeted CRISPR/Cas9 lipid nanoparticles elicits therapeutic genome editing in Head and Neck Cancer, Advanced Science, 12 (2025) 2411032.

[2] J. Guo, M. Gu, Y. Chen, T. Xiong, Y. Zhang, S. Chen, M. Li, X. Chen, X. Peng, Nucleic acid delivery by lipid nanoparticles for organ targeting, Chin. Chem. Lett., (2025) 110849.

[3] Y. Yuan, Y. Li, G. Li, L. Lei, X. Huang, M. Li, Y. Yao, Intelligent Design of Lipid Nanoparticles for Enhanced Gene Therapeutics, Molecular Pharmaceutics, (2025).

[4] J. Witten, Y. Hu, R. Langer, D.G. Anderson, Recent advances in nanoparticulate RNA delivery systems, Proc. Natl. Acad. Sci. U.S.A., 121 (2024) e2307798120.

[5] Y. Eygeris, M. Gupta, J. Kim, G. Sahay, Chemistry of Lipid Nanoparticles for RNA Delivery, Acc. Chem. Res., 55 (2022) 2–12.

[6] R.E. Birdsall, D. Han, K. DeLaney, A. Kowalczyk, R. Cojocaru, M. Lauber, J.L. Huray, Monitoring stability indicating impurities and aldehyde content in lipid nanoparticle raw material and formulated drugs, J Chromatogr B Analyt Technol Biomed Life Sci, 1234 (2024) 124005.

[7] E. Hemmrich, S. McNeil, Active ingredient vs excipient debate for nanomedicines, Nat. Nanotechnol., 18 (2023) 692–695.

[8] Y. Mousli, M. Brachet, J.L. Chain, L. Ferey, A rapid and quantitative reversed-phase HPLC-DAD/ELSD method for lipids involved in nanoparticle formulations, J. Pharm. Biomed. Anal., 220 (2022) 115011.

[9] M. O'Brien Laramy, D.A. Foley, R.H. Pak, J.A. Lewis, E. McKinney, P.M. Egan, R. Yerabolu, E. Dane, O. Dirat, L. Saunders Gorka, J.R. Martinelli, E.M. Moussa, J. Barthuet, Chemistry, manufacturing and controls strategies for using novel excipients in lipid nanoparticles, Nat. Nanotechnol., (2025) 1–14.

[10] D. Jeschek, G. Lhota, J. Wallner, K. Vorauer-Uhl, A versatile, quantitative analytical method for pharmaceutical relevant lipids in drug delivery systems, Journal of Pharmaceutical and Biomedical Analysis, 119 (2016) 37-44.

[11] M. Varache, M. Ciancone, A.-C. Couffin, Development and validation of a novel UPLC-ELSD method for the assessment of lipid composition of nanomedicine formulation, International Journal of Pharmaceutics, 566 (2019) 11-23.

[12] R. Singh, M. Ajagbe, S. Bhamidipati, Z. Ahmad, I. Ahmad, A rapid isocratic high-performance liquid chromatography method for determination of cholesterol and 1, 2-dioleoyl-sn-glycero-3-phosphocholine in liposome-based drug formulations, Journal of Chromatography A, 1073 (2005) 347-353.

[13] L. Li, J.P. Foley, R. Helmy, Simultaneous separation of small interfering RNA and lipids using ion-pair reversed-phase liquid chromatography, Journal of Chromatography A, 1601 (2019) 145-154.

[14] Z. Zhong, Q. Ji, J.A. Zhang, Analysis of cationic liposomes by reversed-phase HPLC with evaporative light-scattering detection, Journal of pharmaceutical and biomedical analysis, 51 (2010) 947-951.

[15] Ph. Eur. 11.6 chapter 2.4.22-2, Composition of fatty acids by gas chromatography, EDQM (Strasbourg, France).

[16] Ph. Eur. 11.6 chapter 2.2.29, Liquid chromatography, EDQM (Strasbourg, France).

[17] Ph. Eur. 11.6 chapter 2.4.22, Composition of fatty acids by gas chromatography, EDQM (Strasbourg, France).

[18] R.A. Frieler, D.J. Mitteness, M.Y. Golovko, H.M. Gienger, T.A. Rosenberger, Quantitative determination of free glycerol and myo-inositol from plasma and tissue by high-performance liquid chromatography, J Chromatogr B Analyt Technol Biomed Life Sci, 877 (2009) 3667-3672.

[19] D. Ilko, A. Braun, O. Germershaus, L. Meinel, U. Holzgrabe, Fatty acid composition analysis in polysorbate 80 with high performance liquid chromatography coupled to charged aerosol detection, Eur J Pharm Biopharm, 94 (2015) 569-574.

[20] V. Matyash, G. Liebisch, T.V. Kurzchalia, A. Shevchenko, D. Schwudke, Lipid extraction by methyl-tert-butyl ether for high-throughput lipidomics, Journal of lipid research, 49 (2008) 1137-1146.

[21] European Directorate for the Quality of Medicines (EDQM), 2.4.22. Composition of fatty acids by GC, in: European Pharmacopoeia, European Directorate for the Quality of Medicines (EDQM),, Strasbourg, France, 2024.

[22] J.H. Gross, Massenspektrometrie : ein Lehrbuch, Springer Spektrum, Berlin, Heidelberg, 2013.

[23] A.T. Jackson, H.T. Yates, J.H. Scrivens, G. Critchley, J. Brown, M.R. Green, R.H. Bateman, The application of matrix-assisted laser desorption/ionization combined with collision-induced dissociation to the analysis of synthetic polymers, Rapid Communications in Mass Spectrometry, 10 (1996) 1668-1674.

[24] B. Wan, J.V. Andhariya, Q. Bao, Y. Wang, Y. Zou, D.J. Burgess, Effect of polymer source on in vitro drug release from PLGA microspheres, Int J Pharmaceut, 607 (2021) 120907.

[25] M. Danaei, M. Dehghankhold, S. Ataei, F. Hasanzadeh Davarani, R. Javanmard, A. Dokhani, S. Khorasani, M.R. Mozafari, Impact of Particle Size and Polydispersity Index on the Clinical Applications of Lipidic Nanocarrier Systems, Pharmaceutics, 10 (2018).

[26] C. Auch, M. Harms, K. Mader, How changes in molecular weight and PDI of a polymer in amorphous solid dispersions impact dissolution performance, Int J Pharmaceut, 556 (2019) 372-382.

[27] J. Herzberger, K. Niederer, H. Pohlit, J. Seiwert, M. Worm, F.R. Wurm, H. Frey, Polymerization of ethylene oxide, propylene oxide, and other alkylene oxides: synthesis, novel polymer architectures, and bioconjugation, Chemical reviews, 116 (2016) 2170-2243.

[28] Ph. Eur. 11.6 monograph 0495, Glycerol monostearate 40-55, EDQM (Strasbourg, France).

[29] Ph. Eur. 11.6 monograph 1429, Glycerole monolinoleate, EDQM (Strasbourg, France).

[30] Ph. Eur. 11.6 monograph 1430, Glycerol mono-oleate, EDQM (Strasbourg, France).

[31] L. Zhang, B.Y.L. Seow, K.H. Bae, Y. Zhang, K.-C. Liao, Y. Wan, Y.Y. Yang, Role of PEGylated lipid in lipid nanoparticle formulation for in vitro and in vivo delivery of mRNA vaccines, J. Controlled Release, 380 (2025) 108–124.

[32] R. John, J. Monpara, S. Swaminathan, R. Kalhapure, Chemistry and Art of Developing Lipid Nanoparticles for Biologics Delivery: Focus on Development and Scale-Up, Pharmaceutics, 16 (2024) 131.

[33] C. Hald Albertsen, J.A. Kulkarni, D. Witzigmann, M. Lind, K. Petersson, J.B. Simonsen, The role of lipid components in lipid nanoparticles for vaccines and gene therapy, Adv. Drug Delivery Rev., 188 (2022) 114416.

[34] G.B. Schober, S. Story, D.P. Arya, A careful look at lipid nanoparticle characterization: analysis of benchmark formulations for encapsulation of RNA cargo size gradient, Sci. Rep., 14 (2024) 1–10.

[35] J.A. Kulkarni, J.L. Myhre, S. Chen, Y.Y.C. Tam, A. Danescu, J.M. Richman, P.R. Cullis, Design of lipid nanoparticles for in vitro and in vivo delivery of plasmid DNA, Nanomed. Nanotechnol. Biol. Med., 13 (2017) 1377–1387.

[36] S.M. Lee, Q. Cheng, X. Yu, S. Liu, L.T. Johnson, D.J. Siegwart, A Systematic Study of Unsaturation in Lipid Nanoparticles Leads to Improved mRNA Transfection In Vivo, Angew. Chem. Int. Ed., 60 (2021) 5848–5853.

[37] Y. Park, J.-W. Park, Preparation, characterization, and stability of lipid nanoparticles including unsaturated lipids, Tenside, Surfactants, Deterg., 60 (2023) 594–598.

[38] M. Kamiya, M. Matsumoto, K. Yamashita, T. Izumi, M. Kawaguchi, S. Mizukami, M. Tsurumaru, H. Mukai, S. Kawakami, Stability Study of mRNA-Lipid Nanoparticles Exposed to Various Conditions Based on the Evaluation between Physicochemical Properties and Their Relation with Protein Expression Ability, Pharmaceutics, 14 (2022) 2357.

[39] A.C. Braun, D. Ilko, B. Merget, H. Gieseler, O. Germershaus, U. Holzgrabe, L. Meinel, Predicting critical micelle concentration and micelle molecular weight of polysorbate 80 using compendial methods, Eur J Pharm Biopharm, 94 (2015) 559-568.

[40] ter Mors et al., Comparison of polysorbate 20 qualities, pharmind, (2020).

[41] K. Schilling, R. Pawellek, K. Lovejoy, T. Muellner, U. Holzgrabe, Influence of charged aerosol detector instrument settings on the ultra-high-performance liquid chromatography analysis of fatty acids in polysorbate 80, Journal of Chromatography A, 1576 (2018) 58-66.

[42] ICH, Validation of analytical procedures Q2 (R2), ICH: Geneva, Switzerland, (2022).

[43] A. Soliven, I.A. Haidar Ahmad, J. Tam, N. Kadrichu, P. Challoner, R. Markovich, A. Blasko, A simplified guide for charged aerosol detection of non-chromophoric compounds-Analytical method development and validation for the HPLC assay of aerosol particle size distribution for amikacin, J Pharm Biomed Anal, 143 (2017) 68-76.

[44] S. Almeling, D. Ilko, U. Holzgrabe, Charged aerosol detection in pharmaceutical analysis, Journal of pharmaceutical and biomedical analysis, 69 (2012) 50-63.

[45] R. Pawellek, T. Muellner, P. Gamache, U. Holzgrabe, Power function setting in charged aerosol detection for the linearization of detector response - optimization strategies and their application, J Chromatogr A, 1637 (2021) 461844.

[46] Ph. Eur. 11.6 chapter 5.10, Control of impurities in substances for pharmaceutical use, EDQM (Strasbourg, France).

[47] Ph. Eur. 11.6 monograph 2034, Substances for pharmaceutical use, EDQM (Strasbourg, France).

[48] R. Pawellek, J. Krmar, A. Leistner, N. Djajić, B. Otašević, A. Protić, U. Holzgrabe, Charged aerosol detector response modeling for fatty acids based on experimental settings and molecular features: a machine learning approach, Journal of Cheminformatics, 13 (2021) 1-14.

[49] B. Behrens, M. Baune, J. Jungkeit, T. Tiso, L.M. Blank, H. Hayen, High performance liquid chromatography-charged aerosol detection applying an inverse gradient for quantification of rhamnolipid biosurfactants, Journal of Chromatography A, 1455 (2016) 125-132.

[50] T. Gorecki, F. Lynen, R. Szucs, P. Sandra, Universal response in liquid chromatography using charged aerosol detection, Analytical Chemistry, 78 (2006) 3186-3192.

[51] Z. Wang, Q. Zhang, H. Shen, P. Yang, X. Zhou, Optimized MALDI-TOF MS Strategy for Characterizing Polymers, Front Chem, 9 (2021) 698297.

[52] K.J. Wu, R.W. Odom, Peer reviewed: characterizing synthetic polymers by MALDI MS, Analytical chemistry, 70 (1998) 456A-461A.

[53] X. He, T.J. Payne, A. Takanashi, Y. Fang, S.D. Kerai, J.P. Morrow, H. Al-Wassiti, C.W. Pouton, K. Kempe, Tailored Monoacyl Poly(2-oxazoline)- and Poly(2-oxazine)-Lipids as PEG-Lipid Alternatives for Stabilization and Delivery of mRNA-Lipid Nanoparticles, Biomacromolecules, 25 (2024) 4591–4603.

[54] S. Li, Y. Hu, A. Li, J. Lin, K. Hsieh, Z. Schneiderman, P. Zhang, Y. Zhu, C. Qiu, E. Kokkoli, T.H. Wang, H.Q. Mao, Payload distribution and capacity of mRNA lipid nanoparticles, Nat Commun, 13 (2022) 5561.

[55] C. Strong, J. Leung, E. Kang, K.E. Badior, M. Robertson, N. Pereyra, E.M. Rowe, A. Wietrzny, B. Ma, Z. Noronha, D. Arnold, M.A. Ciufolini, D.V. Devine, E. Jan, P.R. Cullis, C.J. Kastrup, Genetic engineering of transfusable platelets with mRNA-lipid nanoparticles is compatible with blood banking practices, Blood, 144 (2024) 2223-2236.

[56] V. Bender, L. Fuchs, R. Süss, RP-HPLC-CAD method for the rapid analysis of lipids used in lipid nanoparticles derived from dual centrifugation, International Journal of Pharmaceutics: X, 7 (2024) 100255.

[57] N. Beckert, A. Dietrich, J. Hubbuch, RP-CAD for Lipid Quantification: Systematic Method Development and Intensified LNP Process Characterization, Pharmaceuticals, 17 (2024) 1217.

[58] X. Yu, C. Yu, X. Wu, Y. Cui, X. Liu, Y. Jin, Y. Li, L. Wang, Validation of an HPLC-CAD Method for Determination of Lipid Content in LNP-Encapsulated COVID-19 mRNA Vaccines, Vaccines, 11 (2023) 937.